Printed N'S-MXene@C/Cu Micro-Supercapacitors with Cryo-Tolerant Hydrogel for Wireless Self-Powered Motion Monitoring

Guo-Tao Xiang[a], Rui-Dong Shi[a], Na Chen[a], Jia-Lei Xu[a], Anna Lipovka[b], Raul D. Rodriguez[b], and Jin-Ju Chen[a]*

[a] *School of Materials and Energy, University of Electronic Science and Technology of China, Chengdu 610054, PR China*

[b] *Tomsk Polytechnic University, Lenina Ave. 30, 634034 Tomsk, Russia*

Address correspondence to Jin-Ju Chen, jinjuchen@uestc.edu.cn

1. Experimental Section

1.1 Preparation of flexible micro-supercapacitors (MSCs)

Synthesis of MXene ($Ti_3C_2T_x$): All chemicals were reagent grade and used without further purification. Firstly, 3 g of Ti_3AlC_2 and 1.98 g of LiF were added to 50 mL of concentrated HCI and stirred vigorously at 45°C for 24 h. The resulting precipitates were collected by centrifugation. To further remove the Al layer, the precipitates were then immersed in a 45% HF solution and stirred at 55°C for 12 h. The bottom solid was collected after centrifugation with deionized water and alcohol rinsing for several times. Subsequently, the wet precipitate was resuspended in deionized water, treated with pulsed sonication for 1 h, and centrifuged at 2000 rpm for 30 min to remove large particles. Finally, a homogeneous black supernatant was obtained by centrifugation at 3500 rpm for 1 h.

Preparation of N'S-MXene@C ink: N'S-MXene@C was synthesized through a two-step process involving thiourea intercalation and annealing to incorporate sulfur and nitrogen into the MXene structure. Initially, 500 mg of MXene was dispersed in 50 mL of water containing 500 mg of dissolved and stirred in an ice bath for 30 min.

Following freeze-drying, the thiourea-intercalated MXene was transferred to a tube furnace and annealed at 500 °C for 2 h under the Ar/N_2 atmosphere, with a heating rate of 5 °C min^{-1}. Subsequently, impurities were removed by washing with deionized water to yield N'S-MXene, which was then freeze-dried for 24 h before being stored.

Dissolve 200 mg of glucose in 30 mL of ultrapure water and heat at 85 °C for 20 minutes (until a clear solution is obtained). After cooling to ambient temperature, an aliquot (20 mL) of glucose solution was added to N'S-MXene (1.0 mg mL^{-1}) and heated hydrothermally at 180 °C for 10 h. Finally, the product was collected by centrifugation for 15 min, and the final product was freeze-dried to yield N'S-MXene@C.

The resulting product was dissolved in ethanol and sonicated to create a dispersion. The dispersion was subjected to alternating centrifuged washing with N-methylpyrrolidone (NMP) and ethanol (several cycles). After the final centrifugation with NMP at 2500 rpm for 30 min, the desired ink was collected by decanting the supernatant liquid.

Inkjet printing for the preparation of MSCs electrodes: To prevent clogging of the printheads by large particles, the N'S-MXene@C ink should be filtered through an 800 nm syringe filter before being loaded into the inkjet printer. Subsequently, the ink was deposited on pre-defined copper interdigital electrodes coated on Teslin paper for 25 printing passes to fabricate the planar MSCs electrodes.

1.2 Preparation of PVA/LiCl-EG hydrogels

PVA/LiCl hydrogels were prepared using a repeated freeze-thawing method. Briefly, 20 wt% PVA was added to a LiCl solution with a concentration gradient of 5

M, where the solvent was a mixture of deionized water and ethylene glycol in a 4:1 volume ratio. The mixture was heated to 95°C and kept under mechanical stirring for 2 h. High-speed centrifugation was employed to remove air bubbles, resulting in a homogeneous solution. This solution was then transferred to a silica gel mold and subjected to three freeze-thaw cycles to yield the PVA/LiCl-EG hydrogels.

1.3 Characterization

The morphologies and microstructures of samples were characterized by scanning electron microscopy (SEM, FEI Quanta FEG250, USA) and transmission electron microscopy (TEM, FEI Tecnai F20, USA). X-ray diffraction (XRD, Bruker D8 Advance, Germany) using Cu Ka radiation (λ=0.15418 nm) was applied to study the phases, crystallinity, and structures of samples. The elemental species and chemical states of samples were assessed by X-ray photoelectron spectroscopy (XPS, Thermo Thermo Escalab 250Xi, USA). Fourier transform infrared spectroscopy (FTIR, Bruker Vertex 70, Germany) was employed to analyze the chemical bonding composition of hydrogels. Nitrogen adsorption–desorption isotherms were performed to investigate the specific surface area and porosity information for the as-prepared samples (Micromeritics ASAP 2020 HD88, USA). The Nano Particle Size and Zeta Potential Analyzer (Malvern Zetasizer Nano ZS90, USA) was used to measure the size of the particles as well as the zeta potential for characterizing and judging the particle size distribution and stability of inks. The Atomic Force Microscope (Bruker Dimension ICON) was used to test the morphology and roughness of material surfaces.

2. Electrochemical measurement

During the electrochemical test, MSCs were encapsulated with the Kapton tape. Their electrochemical performances were evaluated using cyclic voltammetry (CV) curves, galvanostatic charge/discharge (GCD) profiles in the voltage range of 0-0.6 V, and electrochemical impedance spectroscopy (EIS) from 0.01 Hz to 100 kHz with an AC amplitude of 5 mV on an electrochemical workstation (Chenhua CHI 660E, China).

Mechanical properties were measured with a universal material testing machine (CMT 6503, MTS/SANS, China). The crosshead speed was fixed at 100 mm min^{-1} for both normal and cyclic tensile tests, using a 1 kN force. The sensing characteristics of hydrogel sensors were tested with a computer-controlled system consisting of a digital multimeter (Keysight 34470A) and a tensile tester (TM2101-T5).

EIS tests of hydrogels were conducted from 100 kHz to 0.01 Hz at amplitude of 5 mV, and the ionic conductivity was calculated as follows:

$$\sigma = \frac{L}{R \cdot S} \quad (1)$$

where S (cm^2) is the cross-sectional area of the hydrogel; L (cm)is the thickness of the hydrogel, and R (Ω) is the bulk resistance (determined from the x-intercept of the EIS plot).

Based on CV curves, the areal capacitance (C_A, mF cm^{-2}) of MSCs was calculated using the following equation (2):

$$C_A = \frac{4}{\upsilon A(V_f - V_i)} \int_{V_i}^{V_f} I(V)dV \quad (2)$$

where υ is the scan rate (V s^{-1}), A is the total area of two electrodes (cm^2), V_f and V_i represent the high and low potential of the CV curves, respectively, and $I(V)$ is the

discharge current (mA).

The areal energy density (E_{areal}, mWh cm^{-2}) of MSCs were evaluated based on the following equation (3):

$$E_{areal} = \frac{1}{2} \times C_A \times \frac{(\Delta V)^2}{3600} \quad (3)$$

where ΔV is the voltage window.

The sensitivity of hydrogel sensors defined as the gauge factor (GF) was calculated using the equation (4):

$$GF = \frac{\Delta R}{\varepsilon R_0} \quad (4)$$

where ΔR is the resistance change with strain, R_0 is the initial resistance prior to strain, and ε is the applied strain.

3. Calculation details

Molecular Dynamics Simulations: Classical molecular dynamics simulations were performed using the Forcite [1], using Condensed Molecular Potential for Atomistic Simulation Studies II (COMPASS II) force-field variables [2]. The LiCl (5 M) electrolyte model contains 360 H_2O, 32 ED, 40 Li^+, and 40 Cl^- molecules. The simulation process was detailed as following: To obtain an equilibrium structure, geometry optimization was carried out in Forcite module using smart algorithm with a convergence level of 0.0001 kcal/mol, where the long-range coulomb interactions and van der Waals interactions were treated by Ewald summation and atom-based summation, respectively. NPT ensemble was used to pre-equilibrate the system, and different temperature (243.15, 273.15, 298.15, and 333.15 K) simulation conditions

were set, maintaining the pressure at 1 atm. Then, atomic simulation was further performed for 50 ns, and simulation trajectories were recorded at an interval of 100 fs for further structural and dynamical analysis.

Density Functional Theory (DFT) Calculations: The electrostatic potential (ESP) configuration of the solvated shell was obtained from the Dmol3 program [3]. For binding energy calculation section, structural optimization was performed at the GGA/PBE level. The localized double-numerical quality basis set with a polarization p-function (DNP-4.4 file) was chosen to expand the wave functions [4,5]. Calculations related to the interactions between different particles were performed using the Dmol3 program module. All calculations, including geometry optimization and electronic density, were performed under periodic boundary conditions, and the convergence of the energy, the maximum force, and the maximum displacement were set to 2×10^{-5} Ha, 2×10^{-3} Ha/Å, and 5×10^{-3} Å, respectively. The binding/desolvation energies between different particles were defined by the following equation of $E = E_{ab} - E_a - E_b$, where E_{ab} (eV) is the total energy of the combination, and E_a and E_b (eV) represent the different parts of the total energy before combination.

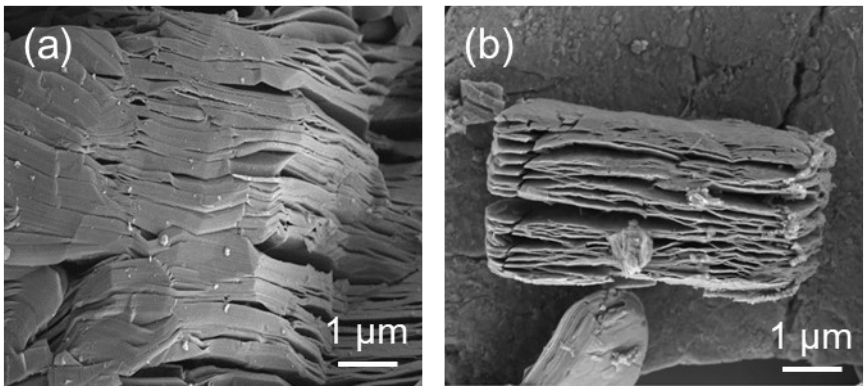

Figure S1. Scanning electron microscopy (SEM) images of MXene nanosheets before and after exfoliation.

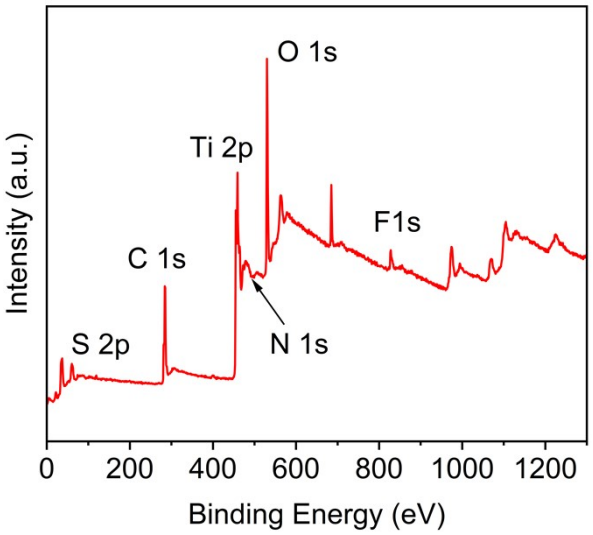

Figure S2. XPS Full spectrum of N'S-MXene@C.

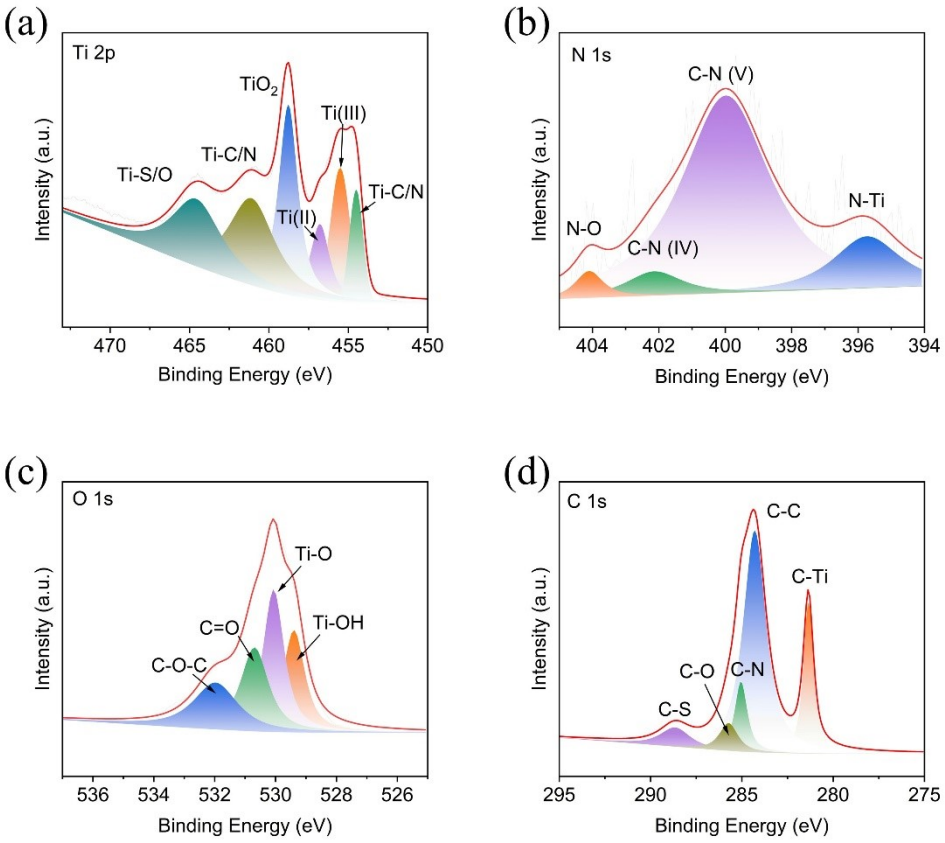

Figure S3. High-resolution XPS spectra of (a) Ti, (b)N 1s, (c) O 1s, and (d) C 1s.

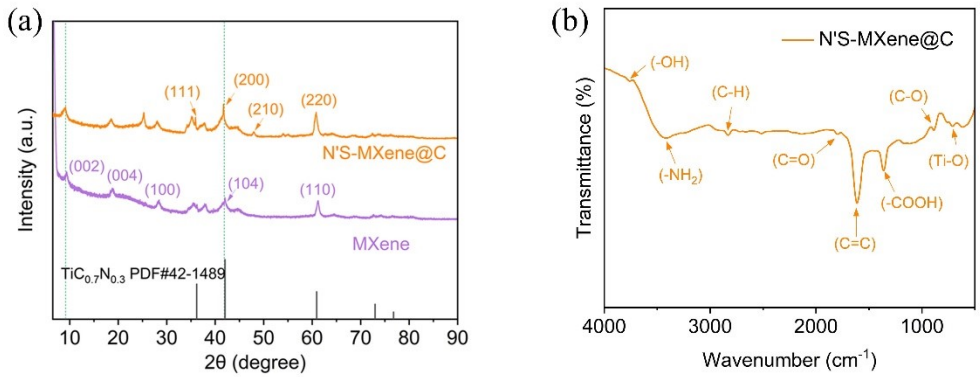

Figure S4. (a)XRD patterns of MXene and N'S-MXene@C and (b) Fourier-transform infrared spectroscopy analysis of N'S-MXene@C

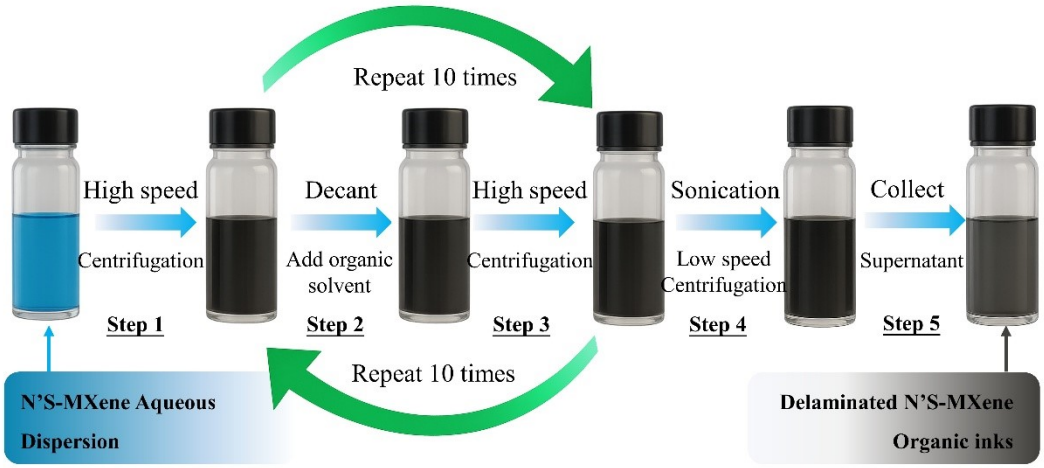

Figure S5. Scheme of organic ink preparation.

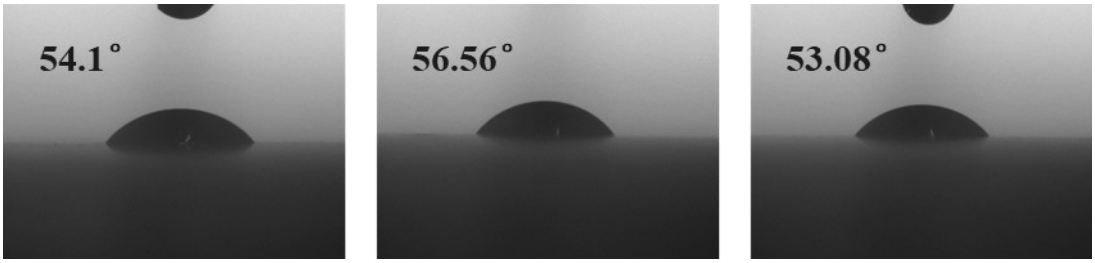

Figure S6. Optical photographs of contact angle with N’S-MXene@C ink

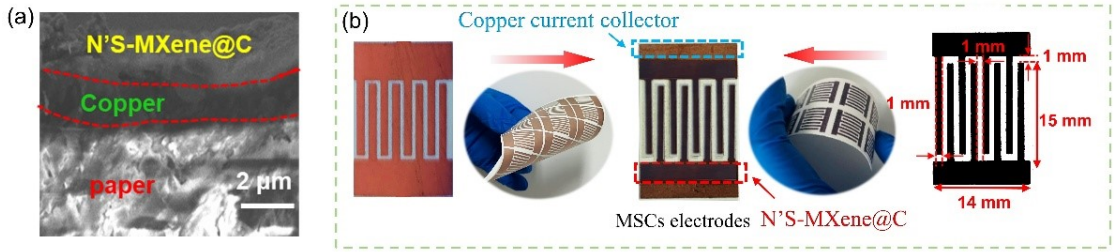

Figure S7. (a) Cross-sectional SEM morphology of the N'S-MXene@C/Cu electrode. (b) Optical and microscopic photographs of the N'S-MXene@C/Cu interdigital electrode.

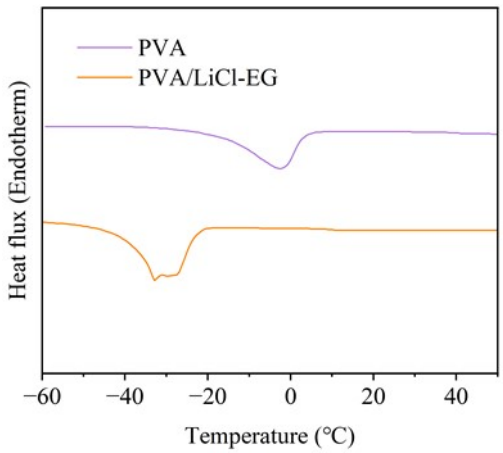

Figure S8. differential scanning calorimetry (DSC) to quantify the freezing transition of the PVA and PVA/LiCl–EG hydrogel

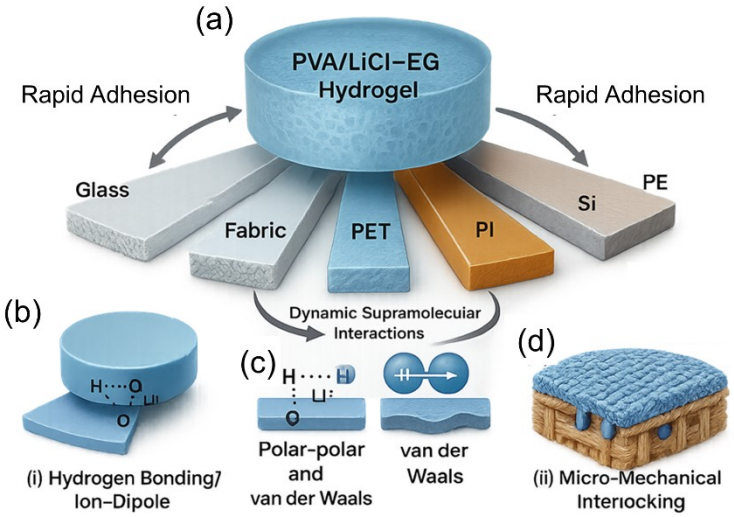

Figure S9. The schematic summarizes that PVA/LiCl–EG adheres rapidly to glass, fabric, PET, PI, ceramic, Si, and PE

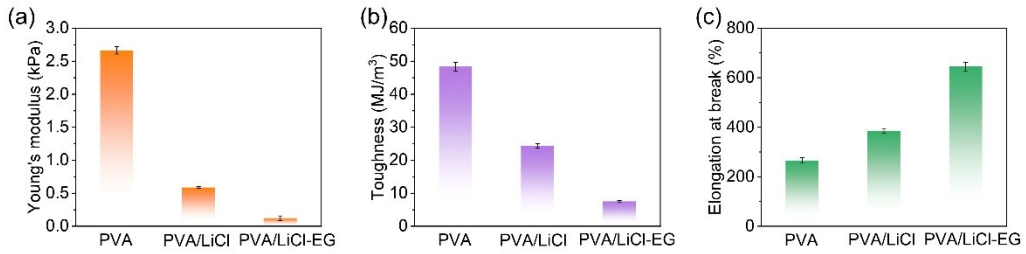

Figure S10. (a) Young's modulus comparison, (b)the toughness and (c) maximum elongation at break of PVA, PVA/LiCl, and PVA/LiCl-EG hydrogels.

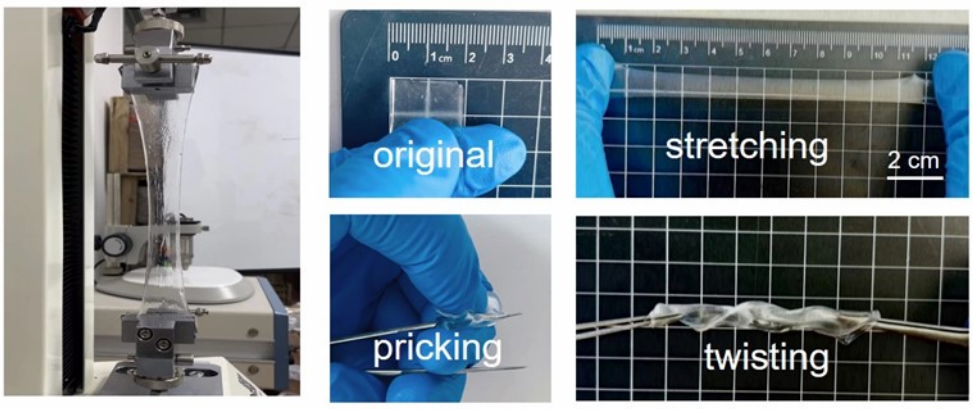

Figure S11. Optical images of the PVA/LiCl-EG hydrogel under different deformation states such as stretching, pricking, and twisting.

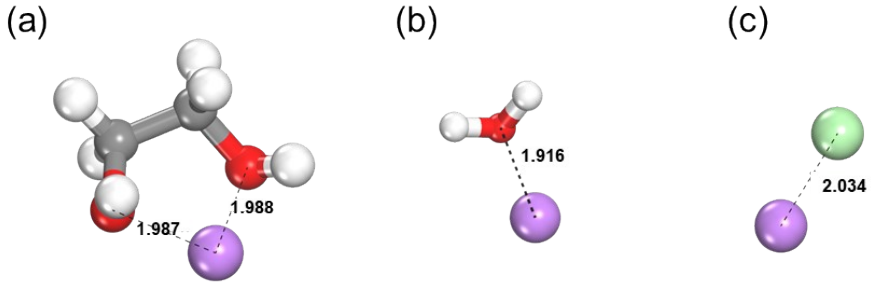

Figure S12. Strength of Li^+ solvated structures with (a) EG, (b) H_2O, (c) Cl^-.

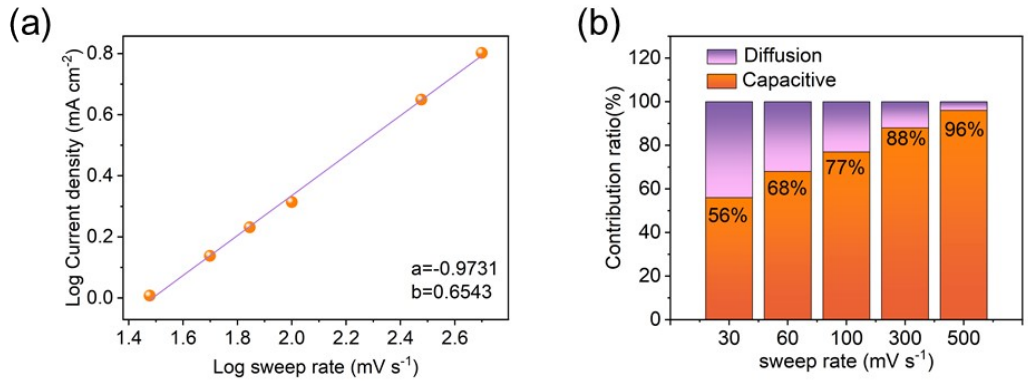

Figure S13 (a) Linear fitting curves of the CV profiles; (b)The contribution ratio of capacitive and diffusion-controlled processes at different scan rates.

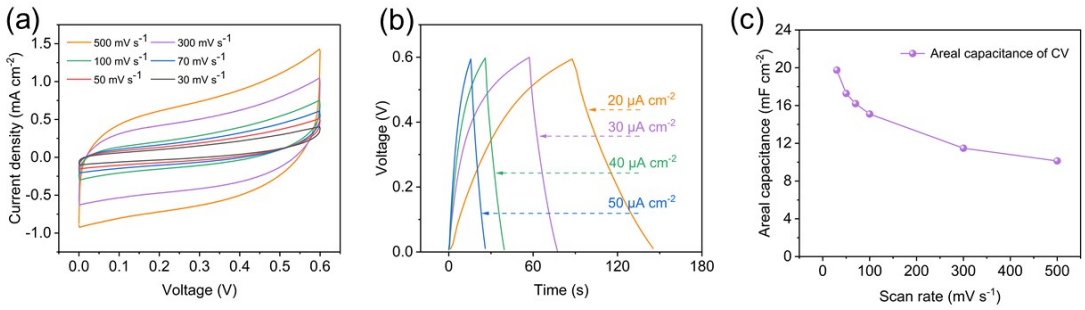

Figure S14. Electrochemical performance of N'S-MXene@C MSCs: (a) CV and (b) GCD.

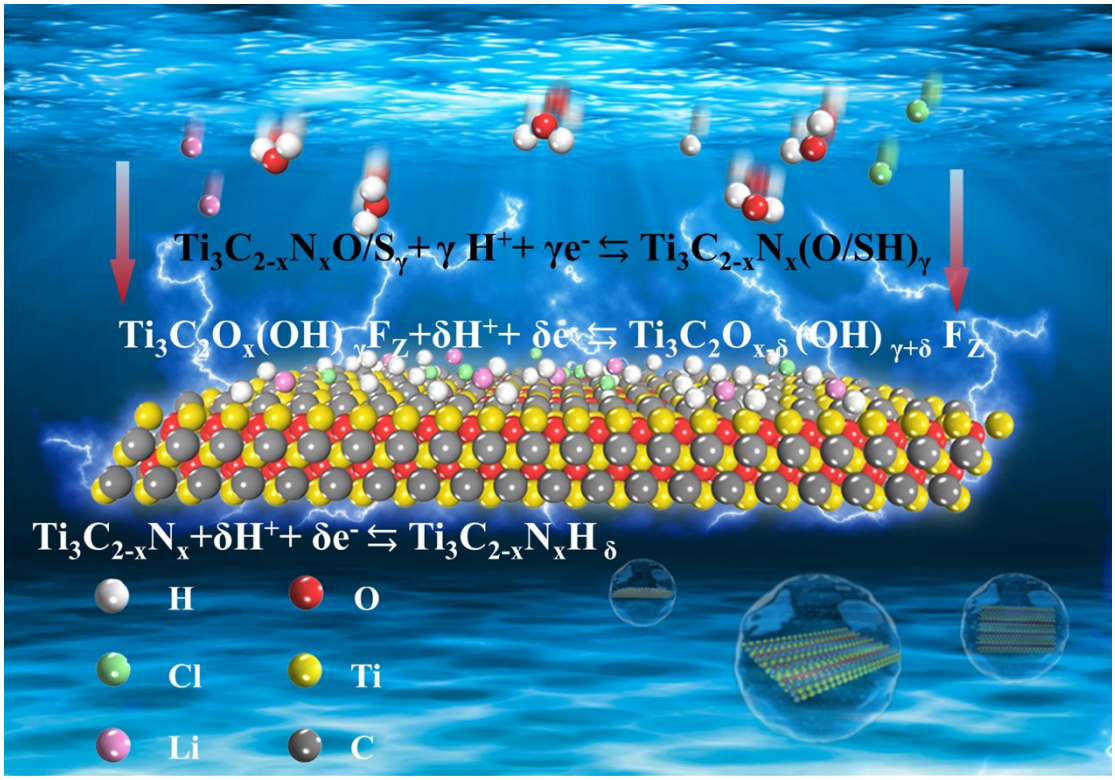

Figure S15. Reversible oxidation-reduction reaction mechanism for the N'S-MXene@C/Cu MSCs.

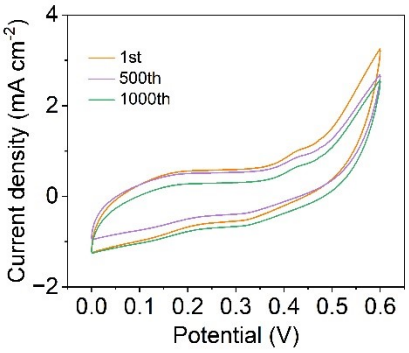

Figure S16. CV curves of the microsupercapacitor after 1000 stretching–releasing cycles.

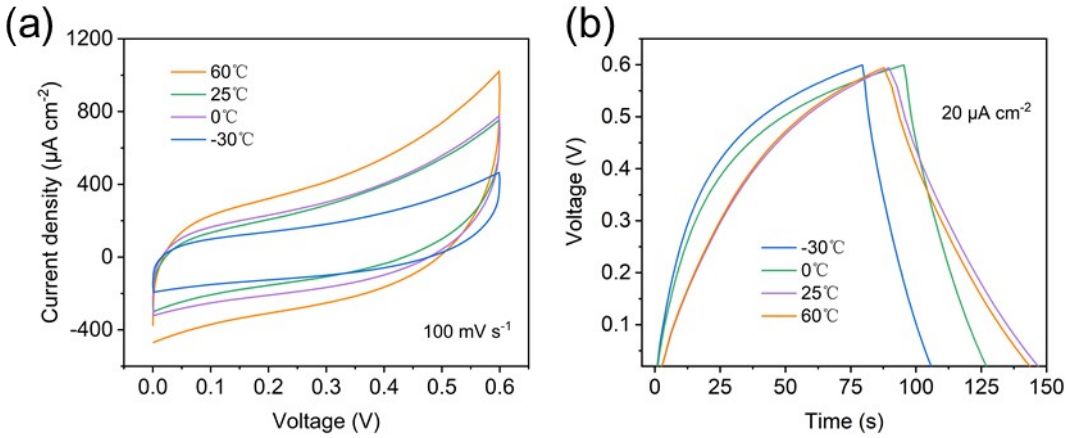

Figure S17. (a) CV curves, (b) GCD curves of N'S-MXene@C MSCs tested at different temperatures.

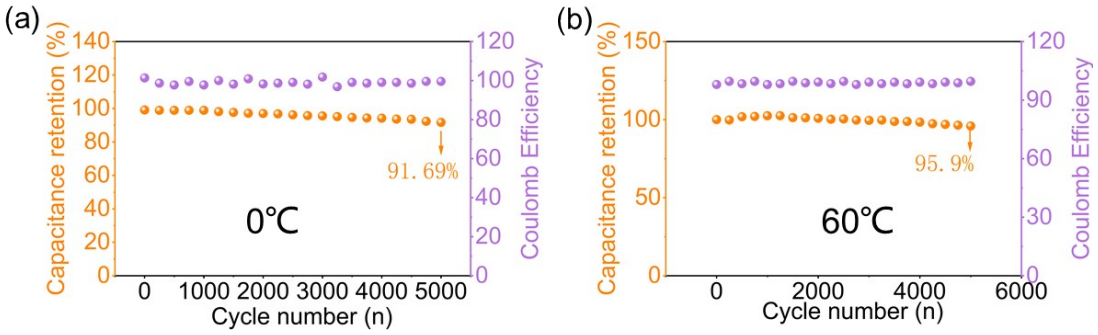

Figure S18. Cycling stability assessments conducted at various temperatures of (a) 0°C and (b) 60°C.

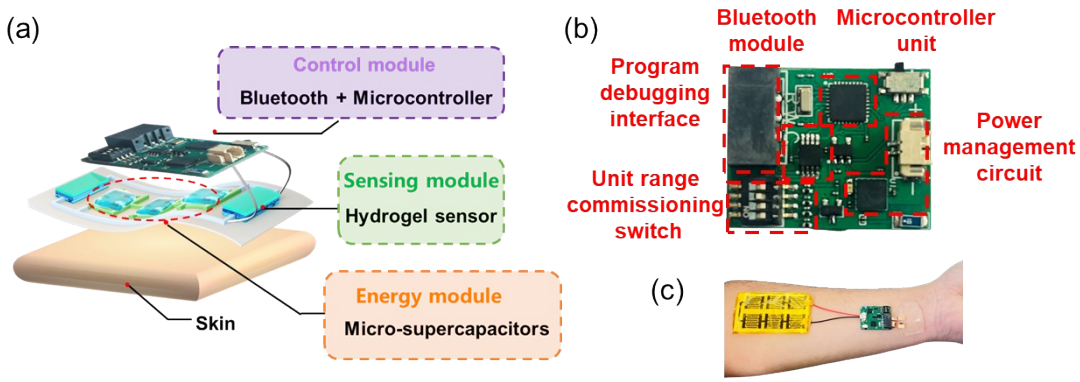

Figure S19. (a) The schematic diagram of the wearable sensing system. (b) Composition of PCB board structure design. (c) Optical images of the self-powered integrated system.

Table S1 Formulation of catalytic ink for electroless copper plating.

Chemical reagent	$AgNO_3$	Deionized water	Ethanol	Glycerol	N-Propanol	Glycol
Dosage	1.2 g	13 mL	7 mL	3 mL	9 mL	4 mL

Table S2 Formulation of electroless copper plating solution

Chemical reagent	**Dosage**
$NaKC_4H_4O_6$	24 g/L
$CHN_2Na_2O_8$	2 g/L
$CuSO_4 \cdot 5H_2O$	8 g/L
$NiSO_4 \cdot 6H_2O$	2 g/L
$C_{10}H_8N_2$	10 mg/L
NaOH	10 g/L
37% formaldehyde solution	12 mL/L

Table S3 Performance comparison of hydrogel sensors

Materials	**Gauge factor (tensile)**	**Sensing range (%)**	**Adhesive**	**Anti-freezing Properties**	**Reference**
PVA/EG/WP	2.36	0-531	N/A	Yes	[6]
PAAm/LiCl	0.84	0-40	N/A	Yes	[7]
PAM-BTO/NaCl	2.12	0-500	Yes	No	[8]
PVA/SWCNT	1.51	0-1000	N/A	N/A	[9]
PVA/LiCl-EG	3.01	0-600	Yes	Yes	This work

Table S4 Performance comparison of the MSC devices constructed in this work with those reported in other literature.

Materials	**Areal energy density (μWh cm^{-2})**	**Power density (mW cm^{-2})**	**Areal capacitance (mF cm^{-2})**	**Temperature Tolerance**	**Reference**
(Ni,Co)Se_2 || $Ti_3C_2T_x$ flexible MSC	8.75	0.5	63 (10 mV s^{-1})	25 ℃	[10]
$Ti_3C_2T_x$ MXene / COF hybrid MSC	12.13	0.63	131.46 (50 mV s^{-1})	25 ℃	[11]
MXene ink / printed MSC	12.26	1.093	88.29 (30 mV s^{-1})	25 ℃	[12]
MXene/RGO composite	3.3	0.4	97.4 (20 mV s^{-1})	25 ℃	[13]
MXene/BC	8.03	0.32	111.5 (100 mV s^{-1})	25 ℃	[14]
MXene	3.86	0.12	77.2 (5 mV s^{-1})	25 ℃	[15]
Graphene-CNT	1.36	0.25	9.81(0.05 mA cm^{-2})	25 ℃	[16]
Ultrastretchable MXene MSC	7.65	0.25	185 (2 mV s^{-1})	25 ℃	[17]
MXene/SA-Fe inkjet-printed MSC	8.4	0.0337	123.8 (5 mV s^{-1})	25 ℃	[18]
N'S-MXene@C/Cu	10.93	0.33	218.5 (30 mV s^{-1})	-30－60℃	This work

Table S5. Comparison of room-temperature and low-temperature cycling retention with representative cryogenic/sub-ambient MSCs and related flexible supercapacitors

Materials	**Room-temperature cycling retention**	**Low-temperature cycling retention**	**Reference**
organohydrogel electrolyte/rGO MSCs	80% (1000th)	80.5% after 5000 cycles (-20℃)	[19]
C-C-based MSCs	85.9% (3000th)	77.5% after 3000 cycles (-20℃)	[20]
HGE-MSC	/	85.7% after 15 000 cycles (-30℃)	[21]
Aqueous Graphene Conductive Ink	91.6% (10000th)	80.1% after 5000 cycles (-20℃)	[22]
PEDOT: PSS / activated carbon	88.9% (3000th)	80.1% after 5000 cycles (-30℃)	[23]
N'S-MXene@C/Cu	95.35% (5000th)	81.36% after 5000 cycles (-30℃)	This work

References

[1] G. J. Ackland, Embrittlement and the Bistable Crystal Structure of Zirconium Hydride. Phys. Rev. Lett. 80 (1998) 2233-2236, DOI: 10.1103/PhysRevLett.80.2233

[2] H. Sun, Z. Jin, C. Yang, R. L. C. Akkermans, S. H. Robertson, N. A. Spenley, S. Miller, S. M. Todd. COMPASS II: extended coverage for polymer and drug-like molecule databases. J. Mol. Model., 22 (2016) 1-10, DOI: 10.1007/s00894-016-2909-0

[3] B. Delley. An all-electron numerical method for solving the local density functional for polyatomic molecules. J. Chem. Phys. 92 (1990) 508−517, DOI: 10.1063/1.458452

[4] J.P. Perdew, K. Burke, M. Ernzerhof. Generalized Gradient Approximation Made Simple. Phys. Rev. Lett. 77 (1996) 3865, DOI: 10.1103/PhysRevLett.77.3865

[5] B. Delley. Ground-State Enthalpies: Evaluation of Electronic Structure Approaches with Emphasis on the Density Functional Method. J. Phys. Chem. A 110 (2006) 13632−13639, DOI: 10.1021/jp0653611

[6] Li Z, Liu P, Chen S. High-Strength, Freeze-Resistant, Recyclable, and Biodegradable Polyvinyl Alcohol/Glycol/Wheat Protein Complex Organohydrogel for Wearable Sensing Devices. Biomacromolecules, 2023, 24(8): 3557-3567, DOI: 10.1021/acs.biomac.3c00321

[7] Tian K, Bae J, Bakarich S E. 3D Printing of Transparent and Conductive Heterogeneous Hydrogel–Elastomer Systems. Adv. Mater. 14, 2017: 1604827, DOI: 10.1002/adma.201604827

[8] Xiang G T, Chen N, Lu B. Flexible solid-state Zn-Co MOFs@MXene supercapacitors and organic ion hydrogel sensors for self-powered smart sensing applications. Nano Energy, 2023, 118: 108936, DOI: 10.1016/j.nanoen.2023.108936

[9] Cai W, Wang J, Qian K, Metal–Organic Framework-Based Stimuli-Responsive Systems for

Drug Delivery. Adv. Sci. 2017, 4(2), DOI: 10.1002/advs.201801526

[10] B. Balan, M. Narayanasamy, S.P. Rajendra, Development of Penroseite (Ni,Co)Se_2 and Ti-MXene Inks for Maximizing the Energy Density of Screen-Printed Flexible Microsupercapacitor. Adv. Mater. Technol. 2023, 8, 2301329, DOI: 10.1002/admt.202301329

[11] Y.Khan, V. S. Kale , J. K. Demellawi, Hybrid microsupercapacitors based on $Ti_3C_2T_x$ MXene and covalent organic frameworks. Mater. Today Energy 44 (2024) 101636, https://doi.org/10.1016/j.mtener.2024.101636

[12] G. Wang, R. Zhang, H. Zhang, Aqueous MXene inks for inkjet-printing microsupercapacitors with ultrahigh energy densities. J. Colloid Interface Sci. 645(2023)359–370, https://doi.org/10.1016/j.jcis.2023.04.155

[13] Y. Joa, S. Jic, Y. Kim, Indirect laser photothermal writing of high areal capacitance micro-supercapacitors with expanded thick MXene electrodes. J. of Energy Storage, 97(2024)112746, https://doi.org/10.1016/j.est.2024.112746

[14] Chen X. Li Q. K, Qi J. Y, Laser fabrication of MXene based planar micro-supercapacitors. Front. Chem. 13(2025):1676794. Doi: 10.3389/fchem.2025.1676794

[15] Li S, Shi Q, Li Y. Intercalation of Metal Ions into $Ti_3C_2T_x$ MXene Electrodes for High-Areal-Capacitance Microsupercapacitors with Neutral Multivalent Electrolytes. Adv. Funct. Mater. 2023, 30(40): 2003721, DOI: 10.1002/adfm.202003721

[16] Wang Y, Zhang Y, Wang G. Direct Graphene-Carbon Nanotube Composite Ink Writing All-Solid-State Flexible Microsupercapacitors with High Areal Energy Density. Adv. Funct. Mater. 2023, 30(16): 1907284, DOI: 10.1002/adfm.201907284

[17] Wang M, Feng S, Bai C. Ultrastretchable MXene Microsupercapacitors. Small, 2023, 19,

2300386, DOI: 10.1002/smll.202300386

[18] Wang G, Zhang R, Zhang H. Aqueous MXene inks for inkjet-printing microsupercapacitors with ultrahigh energy densities. J. Colloid Interface Sci. 2023, 645: 359-370, DOI: 10.1016/j.jcis.2023.04.155

[19] X. Hou, Q. Zhang, L.Wang, Low-Temperature-Resistant Flexible Solid Supercapacitors Based on Organohydrogel Electrolytes and Microvoid-Incorporated Reduced Graphene Oxide Electrodes. ACS Appl. Mater. Interfaces. 2021,13,12432−12441, https://doi-org.libproxy1.nus.edu.sg/10.1021/acsami.0c18741

[20] X. Lin, S. Li, X. Li, 3D patterned fabric-based wearable micro-supercapacitor operating at high voltage by electrostatic actuation. npj Flex. Electron. 9, 60 (2025), https://doi.org/10.1038/s41528-025-00435-2

[21] M. Chen, X. Shi, X. Wang, Low-temperature and high-voltage planar micro-supercapacitors based on anti-freezing hybrid gel electrolyte. J. of Energy Chem. 72 (2022) 195–202, https://doi.org/10.1016/j.jechem.2022.04.029

[22] Y. Wang, X. Zhang, Y Zhu, Planar Micro-Supercapacitors with High Power Density Screen-Printed by Aqueous Graphene Conductive Ink. Materials (2024), 17, 4021. https://doi.org/10.3390/ma17164021

[23] Q. Liu, W. Wu, P. Luo, Preparation of Asymmetric Micro-Supercapacitors Based on Laser-Induced Graphene with Regulated Hydrophobicity and Hydrophilicity. Nanomaterials 2025, 15(8), 584, https://doi.org/10.3390/nano15080584